Limnol. Oceanogr., 46(5), 2001, 1158–1170

Anatomy of turbulence in thermally stratified lakes

Amir Etemad-Shahidi[1]
Department of Civil Engineering, Iran University of Science and Technology, P.O. Box 16675-163, Tehran, Iran

Jörg Imberger
Centre for Water Research, University of Western Australia, Nedlands, Western Australia, 6907, Australia

Abstract

Turbulence within the thermocline of two thermally stratified lakes—Lake Biwa, Japan, and Lake Kinneret, Israel—was investigated using a portable flux profiler. This instrument provided high-resolution profiles of temperature, conductivity, and two components of velocity within a measuring volume of approximately 8 mm^3. Each data profile was segmented into statistically stationary segments. A range of properties of the turbulence, including direct estimates of the vertical mass flux, were then calculated for each segment. It was found that turbulence in the thermocline was generally patchy, but within a patch, dissipation levels were relatively high. The turbulent motions were found to be fine grained with small Thorpe scales and a large skewness of the distribution of the displacement scale. This is distinct to that found in the ocean, where shear instability produces large overturns. The measurement showed that the net vertical mass flux in the thermocline was negligible and less than that predicted by Osborn (1980). This is explained by noting that the net buoyancy flux consisted of two opposing parts—a down-gradient irreversible flux due to turbulent mixing and an up-gradient reversible flux due to restratification—that often cancel each other within a segment. The low measured net buoyancy flux within the interior of the lakes suggested that other processes, such as gravitational adjustments and benthic boundary layer processes, should be responsible for the basin-averaged vertical transport in these lakes.

In lakes, thermal stratification influences mixing and is a controlling parameter for the distribution of dissolved and suspended materials, which determine water quality. Solar radiation in lakes leads to the thermal stratification of the water column. On the other hand, surface winds act to mix the water column. The combined action of solar radiation and wind results in a predominantly three-layer thermal structure; a warm surface-mixed layer, a deep cold layer, and a thermal gradient zone called the metalimnion (thermocline) separating the two.

The vertical eddy diffusivity in the interior of lakes and oceans is about 10 times smaller than at the boundaries (Ledwell and Bratkovich 1995; Toole et al. 1995; Wuest et al. 2000). Studies at the interior of basins indicated K_ρ values close to 10^{-5} m^2 s^{-1} (e.g., Jenkins 1980; Ivey 1987; Ledwell and Watson 1991; Ledwell et al. 1993), which is smaller than the value of 10^{-4} m^2 s^{-1} (Munk 1981; Ledwell and Hickey 1995) suggested as a basin average value. One of the reasons for the lower value of vertical eddy diffusivity in the basin interior is that the water column is strongly stratified, and turbulence is quite patchy and intermittent in the thermocline. Therefore, only a fraction of the water column is really turbulent (Gregg 1980; Wuest et al. 2000), and even within the turbulent patches, the displacement scales are small (Imberger and Ivey 1991; Wuest et al. 2000).

Moreover, the value of the vertical eddy diffusivity from microstructure studies is usually estimated indirectly from measurement of the dissipation ε assuming a constant mixing efficiency. This yields the estimate $K_\rho = \lambda\varepsilon/N^2$, where $\lambda \sim 0.2$ (Osborn 1980; Oakey 1982) for shear induced turbulence, and N is the buoyancy frequency. Direct measurements have, however, shown that the flux Richardson number, or mixing efficiency $R_f = \lambda/(1 + \lambda)$, is not constant but depends on the value of the turbulent Froude number (Ivey and Imberger 1991) or the gradient Richardson number (Rohr and Van Atta 1987). The maximum R_f value is about 0.25; hence, the above-mentioned indirect method yields an upper limit of K_ρ.

Experiments have shown that turbulence can sustain a buoyancy flux when $\varepsilon/\nu N^2 > 15$–25, where ν is the kinematic viscosity (e.g., Stillinger et al. 1983; Itsweire et al. 1993). Many attempts have been made to relate mixing efficiency and buoyancy flux to the gradient Richardson number, Ri_g, in shear flows (Rohr and Van Atta 1987; Rohr et al. 1988). Turbulence was suppressed by buoyancy for $Ri_g > 0.21$, and for larger values of Ri_g, up-gradient (U.G.) flux occurred (Yoon and Warhaft 1990; Holt et al. 1992; Itsweire et al. 1993).

Ivey and Imberger (1991) reanalyzed the existing experimental data and showed that the mixing efficiency was mainly a function of Fr_t, the turbulent Froude number, with a maximum efficiency of 0.25 at $Fr_t = 1$. This result was confirmed later by laboratory experiments of Piccirillo and Van Atta (1997) and numerical simulation of Schumann and Gerz (1995). Recently Ivey et al. (1997), using the numerical model of Holt et al. (1992), proposed a set of equations that

[1] Corresponding author (etemad@sun.iust.ac.ir).

Acknowledgments

We are grateful to Michio Kumagai and Tamar Zohary. This study could not have been carried out without the assistance, facilities, and active support of the Lake Biwa Research Institute, Japan, and Y. Alon Kinneret Limnological Laboratory, Israel. We also thank Greg Ivey for his fruitful comments and Angelo Saggio for developing the variable filter used in the date processing.

Center for Water Research Environmental Dynamic reference ED 952 AE.

correlated mixing efficiencies with Fr_t and the turbulent Reynolds number, Re_t.

Recently, Huq and Britter (1995*a*,*b*) noted that the buoyancy flux was often a combination of up-gradient flux and down-gradient (D.G.) flux. In their experiment, nonzero net buoyancy flux resulted from intermittent events with a low frequency of occurrence (*see also* Hannoun and List 1988). All of these results suggest that the buoyancy flux is intermittent and can consist of two competing parts: an U.G. flux and a D.G. flux. The scale at which these contributions occur seems to depend on the nature of the particular event being observed. In addition, the existence of U.G. flux shows that zero net buoyancy flux is necessary, although not sufficient for complete suppression of turbulent mixing (Lienhard and Van Atta 1990).

Measurements of buoyancy flux in the field also indicated that both U.G. and D.G. flux exist in the turbulent events. Limited studies of the oceanic thermocline have reported that weak U.G. flux occurred mostly at the large scale (Yamazaki and Osborn 1993; Fluery and Lueck 1994). However, Moum (1990) and Lemckert and Imberger (1995) found numerous examples with dominant U.G. flux in the ocean and lakes, respectively. Recent extensive study of Moum (1996*a*) showed that the turbulent patches with dominant U.G. flux were as frequent as the patches with dominant D.G. flux. Hence, the net mixing efficiency in the thermocline of the ocean was essentially negligible. On the other hand, measurements of Gargett and Moum (1995) in a tidal channel showed a net mixing efficiency of 0.2.

In spite of the important role of the thermocline in the hydrodynamics and water quality of lakes, no direct measurements of buoyancy flux and dissipation in a lake thermocline exist. The aim of the present contribution is to examine the buoyancy flux and the dissipation associated with the turbulence in the thermocline of strongly stratified lakes and to show that the turbulent events are intermittent with a negligible mean buoyancy flux. With this goal in mind, the turbulent activity in the thermocline of two lakes, Lake Biwa, Japan, and Lake Kinneret, Israel, was investigated during the stratified periods.

Background

Direct method of dissipation measurement and isotropy—The rate of dissipation of turbulent kinetic energy per unit mass is given by (Hinze 1975) as

$$\varepsilon = \nu\overline{\left(\frac{\partial u_i}{\partial x_j} + \frac{\partial u_j}{\partial x_i}\right)\frac{\partial u_j}{\partial x_i}}, \tag{1}$$

where u_i is the ith component of velocity fluctuation, and summation notation is implied by repeated indices. The overbar represents the ensemble average, and the coordinates x_j are oriented so that $j = 3$ is positive upward.

For isotropic incompressible turbulence, Taylor (1935) showed that Eq. 1 can be further simplified to

$$\varepsilon_H = 7.5\nu\overline{\left(\frac{\partial u_1}{\partial x_3}\right)^2}, \tag{2}$$

where ε_H is the isotropic estimation for the dissipation.

Indirect dissipation measurement—Indirect methods are based on the measurement of tracer (usually temperature) gradient microstructure (e.g., Dillon and Caldwell 1980). In these methods, the rate of dissipation is calculated from the roll-off at the high wave numbers of the tracer gradient spectrum. In homogeneous isotropic turbulence, the nondimensional spectrum of a temperature gradient fluctuation is given by (Batchelor 1959; Gibson and Schwarz 1963)

$$S(k) = \left(\frac{Q}{2}\right)^{1/2}\frac{\chi f(\alpha)}{k_B K}, \tag{3}$$

where Q is a constant related to the principal rate of strain, χ is the temperature variance dissipation rate defined as $6K(\partial T'/\partial z)^2$, T' is the temperature turbulent fluctuation, and $f(\alpha)$ is a function defined by

$$f(\alpha) = \alpha(e^{-(1/2)\alpha^2}) - \int_\alpha^\infty e^{-(1/2)\beta^2}\, d\beta. \tag{4}$$

The nondimensional wave number α is defined by $2(Q)^{1/2}k/k_B$, where k_B is the Batchelor wave number $(\varepsilon/\nu K^2)^{1/4}$, and K is the thermal diffusivity. Although the Batchelor spectrum was proposed for isotropic turbulence in unstratified fluid, Dillon and Caldwell (1980) showed that it may be successfully applied to a stratified flow, provided that certain constraints are met. For values of dissipation $>10^{-8}$ m^2 s^{-3}, the estimates from direct and indirect methods agreed by an average factor of two in the ocean and lakes (Oakey 1982; Lemckert and Imberger 1995).

Mixing efficiency—For an incompressible fluid, the turbulent kinetic energy equation may be written as

$$-\frac{\partial}{\partial t}\overline{\left(\frac{q^2}{2}\right)} - \frac{\partial}{\partial x_j}\overline{\left(\frac{u_j q^2}{2}\right)} - \frac{\partial}{\partial x_j}\left(\frac{1}{\rho_0}\overline{u_j p'}\right) - U_j\frac{\partial}{\partial x_j}\overline{\left(\frac{q^2}{2}\right)} - \overline{u_i u_j}\frac{\partial U_i}{\partial x_j} = \frac{g}{\rho_0}\overline{u_3\rho'} + \nu\overline{\frac{\partial u_i}{\partial x_j}\frac{\partial u_i}{\partial x_j}}, \tag{5}$$

where $\overline{q^2}$ is twice the turbulent kinetic energy (TKE) per unit mass, ρ' is the pressure fluctuation, ρ_0 is a reference density, U_j is the mean velocity, and u_j is the fluctuation velocity. Ivey and Imberger (1991) rewrote Eq. 5 in the form

$$m = b + \varepsilon, \tag{6}$$

where m is the rate of production, change, and importation of mechanical energy available for mixing and b is the buoyancy flux. They also generalized the definition of flux Richardson number R_f to read

$$R_f = \frac{b}{b + \varepsilon}. \tag{7}$$

Length scales of turbulence—The state of turbulence can be determined from the ratio of its length scales, which form nondimensional numbers (Imberger 1995). The most important length scales are the Kolmogorov scale (Kolmogorov 1941),

$$L_K = \left(\frac{\nu^3}{\varepsilon}\right)^{1/4}, \tag{8}$$

and the Ozmidov scale (Daugherty 1961; Ozmidov 1965),

$$L_O = \left(\frac{\varepsilon}{N^3}\right)^{1/2}. \tag{9}$$

In field studies using vertical profilers, the Thorpe scale L_T (Thorpe 1977; Dillon 1982) is often measured. The Thorpe scale is the root mean square (rms) value of Thorpe displacements, l_d. Another scale is the centered displacement scale, l_c, which is the Thorpe displacement but displaced and averaged to correspond to the center of an overturn event (Imberger and Boashash 1986).

The turbulent Froude number may be defined by

$$\mathrm{Fr}_t = \frac{q}{NL_T} \approx \left(\frac{\varepsilon}{N^3 L_T^2}\right)^{1/3} = \left(\frac{L_O}{L_T}\right)^{2/3}, \tag{10}$$

the ratio of two of the above-mentioned length scales.

In a linearly stratified flow, Fr_t is equal to the square root of ratio of the TKE and available potential energy of unstable density fluctuations (APEF) (Dillon and Park 1987), as can be seen by

$$\mathrm{Fr}_t = \left(\frac{q^2}{N^2 L_T^2}\right)^{1/2} = \left(\frac{\mathrm{TKE}}{\mathrm{APEF}}\right)^{1/2}, \tag{11}$$

where the generalized definition of APEF is (Dillon and Park 1987)

$$\mathrm{APEF} = \langle g' l_d/2 \rangle, \tag{12}$$

where $g' = g\rho'/\rho_0$ is the effective gravity and $\langle\ \rangle$ designates vertical averaging. Later, we will discuss the relationship between APEF and $N^2L_T^2$.

The turbulent Reynolds number maybe defined as

$$\mathrm{Re}_t = \frac{qL_T}{\nu} \approx \frac{\varepsilon^{1/3} L_T^{4/3}}{\nu} = \left(\frac{L_T}{L_K}\right)^{4/3}. \tag{13}$$

Another nondimensional number that has been used frequently in turbulence classification (e.g., Stillinger et al. 1983; Gibson 1986; Itsweire et al. 1986) is the small-scale Froude number Fr_γ (Luketina and Imberger 1989) defined as

$$\mathrm{Fr}_\gamma = \left(\frac{\varepsilon}{\nu N^2}\right)^{1/2} = \left(\frac{L_O}{L_K}\right)^{4/3}. \tag{14}$$

The critical Fr_γ that can support buoyancy flux is around four for steady grid- and shear-generated turbulence. However, this is not universal and may change as a function of the Reynolds number (Itsweire et al. 1993; Huq and Stretch 1995) and the initial conditions (Piccirilo 1993).

Field programs—Two lakes were selected to investigate the dynamics of turbulence in the thermocline. The first was Lake Biwa, which is the largest fresh water lake in Japan. It is located in the middle of mainland Japan at 35°N 136°E. The area of lake Biwa is 674 km^2, and the lake consists of two basins. The main basin in the north has a maximum depth of 104 m, and the smaller basin in the south has a maximum depth of 8 m (Okuda et al. 1995). It is a monomictic lake with a long mixing period during the winter (Nakanashi et al. 1998).

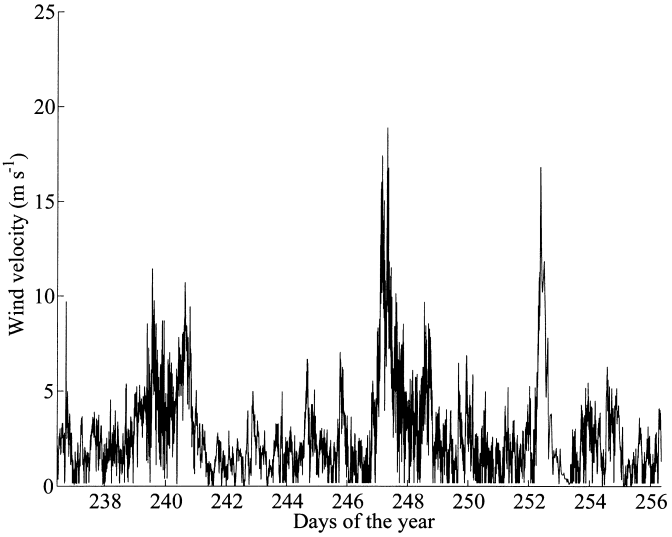

Fig. 1. Wind record from 24 August (day 237) to 13 September 1993 (day 256) with a sampling period of 1 min in Lake Biwa, Japan. The lake experienced three typhoons on days 240, 247, and 252.

The investigation was a part of the Lake Biwa Transport Experiment (BITEX), carried out in 1993 to study the horizontal and vertical transport processes between the south and north basins. Microstructure data were collected from 26 August to 13 September 1993 (days of the year 238–256) at sites 30 to 60 m deep. The sites were concentrated around station BN 50 situated on the slope rising to the southern basin (Saggio and Imberger 1998). The metalimnion in Lake Biwa extended from 12 to 30 m deep, and the water temperature was between 27°C in the surface layer and 8°C in the hypolimnion. The period of the experiment covered part of the typhoon season. Three storms with maximum wind speed of 20 m s^{-1} passed near the lake during the experiment (Fig. 1).

The second investigation site was Lake Kinneret in the North of Israel, located at 33°N 36°E. The lake has an area of 168 km^2 and a maximum depth of 43 m (Saggio and Imberger 2001). The experiment was conducted from 17 to 21 July 1994 (days of the year 198–202). During the experiment, the weather was warm with calm mornings and windy afternoons (Fig. 2). Sampling sites were concentrated over the moderate northwest region of the lake. The water depth at the stations was between 11 and 30 m, and the metalimnion extended between 12 and 22 m deep. The temperature was between 27°C in the surface layer and 18°C in the hypolimnion. In both lakes the measured salinity was nearly constant, and the vertical stratification was due to temperature variations.

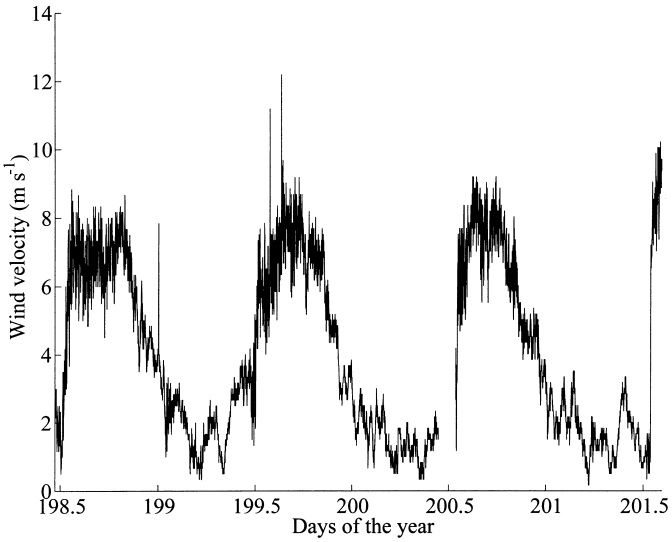

Fig. 2. Wind record from Sta. T20 with sampling period of 1 min in Lake Kinneret, Israel. Note the periodic high wind in the afternoons and calm weather in the mornings.

Instrumentation and data reduction

Microstructure data was collected by using the portable flux profiler (PFP) described in detail by Imberger and Head (1994). The PFP is a battery-powered vertical profiler that can measure two components of velocity, temperature, and conductivity. The PFP is about 1.5 m long (Fig. 3), and its nominal drop velocity is 0.1 m s^{-1}. All data was collected at a frequency of 100 Hz, yielding a spatial resolution of approximately 1 mm.

The temperature sensors were FPO7 thermistors with a response time of 12 ms. Fast-response, four-electrode, conductivity sensors (Head 1983) with a response time of 4 ms were used to measure the conductivity. The resolutions of the temperature and conductivity sensors were 0.001°C and 0.0004 S m^{-1}, respectively. The velocities were measured by a Laser Doppler Anemometry (LDA). The range of the velocities measurements was $\pm$0.20 m s^{-1}, with a 0.001 m s^{-1} resolution (Imberger and Head 1994).

Data reduction—Fourteen profiles from five stations in Lake Biwa and 60 profiles from three stations Kinneret experiments were selected and processed. The criteria for choosing the profiles was that they exhibited a relatively large buoyancy frequency ($N > 5 \times 10^{-3}$ s^{-1}) and good signal to noise ratios.

The steps in the data processing were as follows. The conductivity and temperature signals were sharpened/smoothed (Fozdar et al. 1985) digitally before computing the salinity and density. To determine the stationary segments, a segmentation algorithm was then applied to the temperature gradient signals. Owing to the instrumentation limits, a threshold of $\varepsilon_B = 10^{-10}$ m^2 s^{-3} was chosen to exclude nonactive segments. Two typical profiles with their segments are shown in Fig. 4: one from a quiet profile (Fig. 4a–c) and one from an active profile (Fig. 4d–f).

The density fluctuation ρ', g', and l_d were then calculated

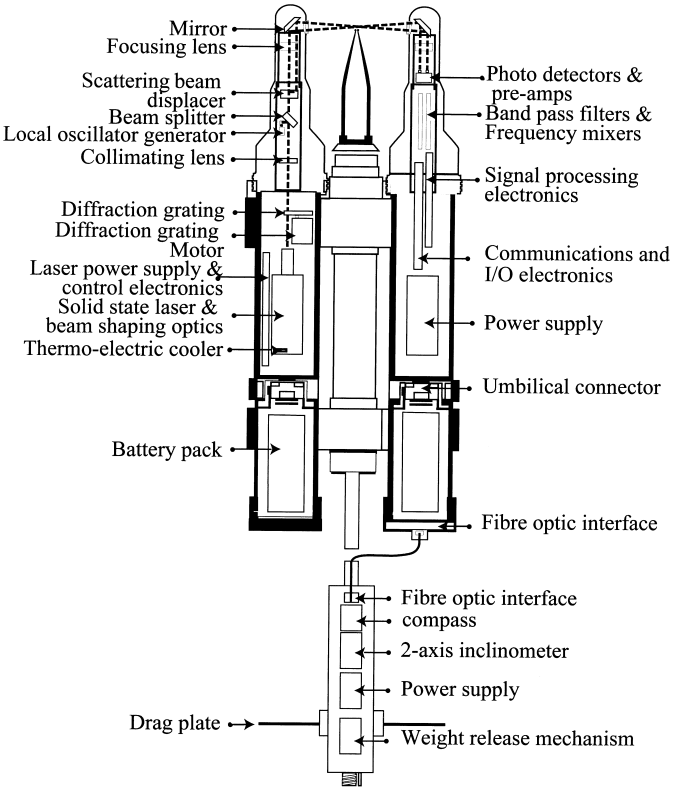

Fig. 3. Schematic of the portable flux profiler (PFP) showing the different parts of the instrument. The length of the probe is 1.5 m and its weight is about 25 kg in the air.

for each point by comparing the recorded profile and the monotonized profile. The length scale l_d was then used to compute L_T and l_c. The symmetry of the distribution of l_c within each segment was determined from the skewness, Sk. The skewness of any variable is the third moment, which is nondimensionalized by the cube of the standard deviation and is given by (e.g., Tennekes and Lumley 1981):

$$\mathrm{Sk} = \frac{\overline{(x - \mu)^3}}{\sigma^3}, \tag{15}$$

where μ is the mean and σ is the standard deviation.

We assumed that scales larger than overturn scales are nonturbulent (Peters et al. 1995; Saggio and Imberger 2000). Therefore, turbulent and nonturbulent velocity fluctuations were distinguished by their length scales and variable-length filtering was used to resolve turbulent fluctuations. This variable filter was then applied to the velocity signal to separate the nonturbulent part of the signal. To remove the high-frequency noise introduced by the mechanical parts, a 32 Hz (320 cpm) filter was also applied to the velocity signals. Finally, the velocity fluctuations within each segment were detrended by removing the mean.

For calculating the segment-averaged buoyancy flux, velocity and density turbulent components were multiplied by each other, averaged over the segment, then multiplied by g/ρ. Given ε and b, the flux Richardson number was calculated from Eq. 7 for each segment.

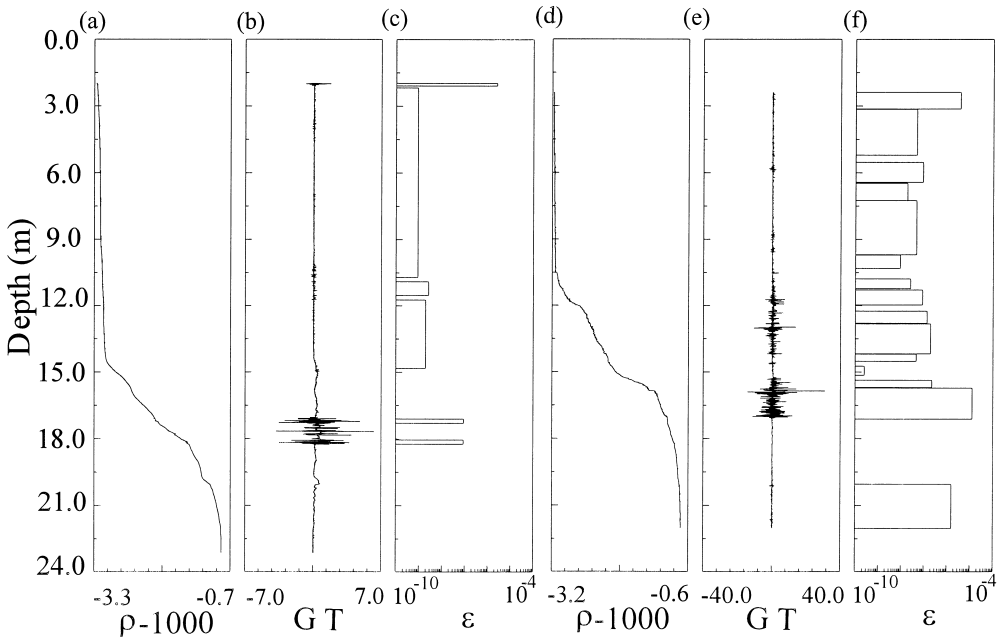

Fig. 4. Microstructure data collected by the PFP descending through the water column at 1121 and 2044 h on day 201 (1994) at Sta. T20 in Lake Kinneret before and after the afternoon's high winds, showing an increase in turbulence. (a) Density profile before high wind. (b) Corresponding vertical gradient of temperature. (c) Stationary segments (rectangles) and their temperature gradient dissipation levels. (d) Density profile after the high wind. (e) Corresponding vertical gradient of temperature. (f) Stationary segments (rectangles) and their dissipation levels.

It is important to note that the profile collected by PFP is a snapshot of the turbulence field at the time of the measurement. Because the velocity scale of the turbulent motions (<0.01 m s^{-1}) was less than the measurement speed (0.1 m s^{-1}), Taylor's frozen turbulence hypothesis was applicable, and vertical averaging was substituted for the ensemble averaging in Eq. 5. However, the buoyancy flux obtained from vertical profilers depends strongly on the time and place of the piercing of a turbulent event (Lemckert and Imberger 1995). Therefore, not surprisingly, the flux obtained for the segments exhibited scattering even for the same values of Fr_t and Re_t. The short-length stationary segments in the thermocline of the lakes also increased the scatter.

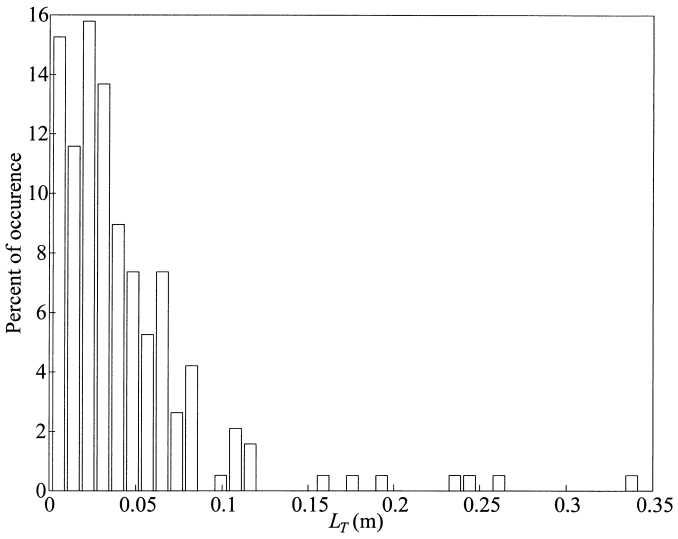

Fig. 5. Histogram of Thorpe scales, L_T for the turbulent segments with $\varepsilon_B > 10^{-10}$ m^2 s^{-3}, showing the relatively small size of overturns in the thermocline.

We assumed that the turbulence was axisymmetric about the vertical axis and the turbulent velocity scale was derived from $(2u_1^2 + u_3^2)^{1/2}$ for each point. The rms of these point values were then used to estimate q, the segment velocity scale.

Results

The nature of the density overturns—The intensity and distribution of the turbulent patches varied greatly from one profile to the next: during periods of little internal wave activity, the profiles tended to yield results, as shown in Fig. 4a–c. In the metalimnion, only two short segments exhibited dissipations $>10^{-10}$ m^2 s^{-3}, and each event was small in vertical extent (Fig. 4d–f). In general when this occurred, the rate of dissipation increased.

The distribution of the size of the overturn events is best seen from the histogram of the Thorpe scale L_T (Fig. 5), in which the frequency of occurrence was plotted against the estimated L_T for each segment. From the figure, it may be noted that the distribution was highly skewed to very small values of L_T. Most of the segments had a value of $L_T < 0.1$ m, close to the previous measurements in the lake thermoclines (Imberger and Ivey 1991; Wuest et al. 2000), but

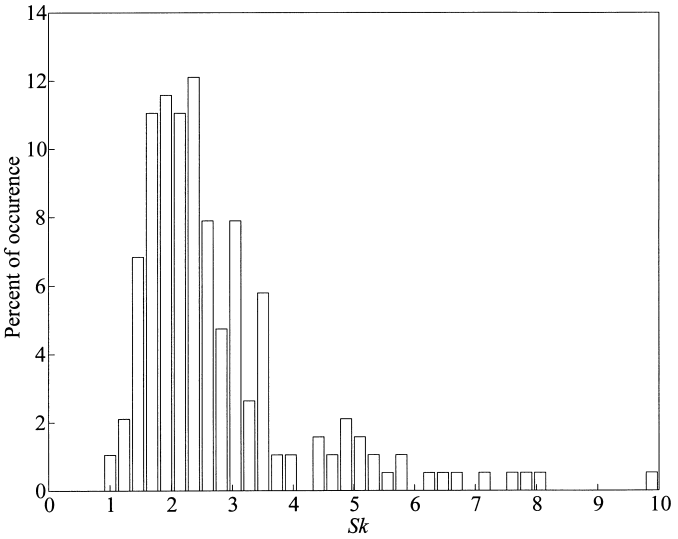

Fig. 6. Histogram of the centered displacement scale skewness, Sk, for the turbulent patches with $\epsilon_B > 10^{-10}$ m^2 s^{-3}, showing that all of the segments had a skewed distribution of l_c.

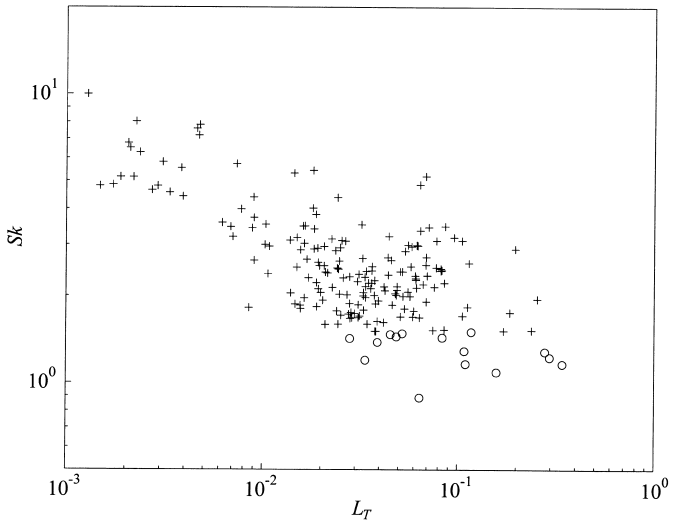

Fig. 7. Skewness of the distribution of l_c within each segment Sk as a function of the Thorpe scale L_T showing an inverse relation between these two parameters. Data points are classified according to the skewness of their centered displacement scale: Sk $\leq$ 1.5 (○) and $Sk > 1.5$ (+).

much smaller than that observed in the ocean, where stratification is weaker and an L_T of several meters is not uncommon (Gregg 1980; Gregg et al. 1986). The average value of L_T was 43 mm, and the median of L_T was 32 mm. Therefore, compared to the oceanic values, the Thorpe scale L_Ts were much smaller.

The characteristics of overturns within a particular turbulent segment may be characterized by the skewness of l_c (Teoh et al. 1997). A positive skewness, Sk, of the length scale distribution indicates that most of the displacement values within the segment are smaller than the mean, and a few large values support the bias of the mean. The histogram of Sk (Fig. 6) showed that all the segments had a positive Sk and more than half of the segments had Sk > 2. Teoh et al. (1997) found a similar skewness range in their laboratory study of internal wave–wave interaction. They argued that the absence of segments with symmetric length scale distributions or distributions with a prevalence with small length scales indicated the absence of the characteristic large-scale shear-driven billows. Further evidence to support this argument was the inverse relationship between Sk and L_T (Fig. 7). Over three decades of L_T, the larger overturns had a smaller had a smaller Sk.

Figure 8 illustrates the histogram of the rms values of the gravity anomalies in each segment, obtained by subtracting the monotonized density profile from the actual density profile. Again, the mean value for all the segments was very small (2.2×10^{-5} m s^{-2}), the distribution was skewed, and the mean was biased by a few larger values ($>1 \times 10^{-4}$ m s^{-2}). The low values of gravity anomaly were also observed by Teoh et al. (1997) when there was no mean shear. All these results led us to the conclusion that the driving mechanism for the bulk of the observed turbulent events was internal wave–wave interaction and not steady shear.

Dissipation of turbulent kinetic energy—As seen in Fig. 4, the dissipation of the turbulent kinetic energy was extremely variable throughout the water column and intermittent in time. Segments with dissipation levels greater than the threshold of 10^{-10} m^2 s^{-3} were relatively small and usually separated by thick quiescent layers. Profiles similar to that shown in Fig. 4e were observed only after the periods of the highest winds, which excited seiching. During other times, the temperature gradient signal showed mostly one-sided excursions indicative of step structures (Fig. 4a,b).

Dissipation for the stationary segments were estimated two ways: indirectly from the temperature gradient signal using Eq. 3 and directly using Eq. 2.

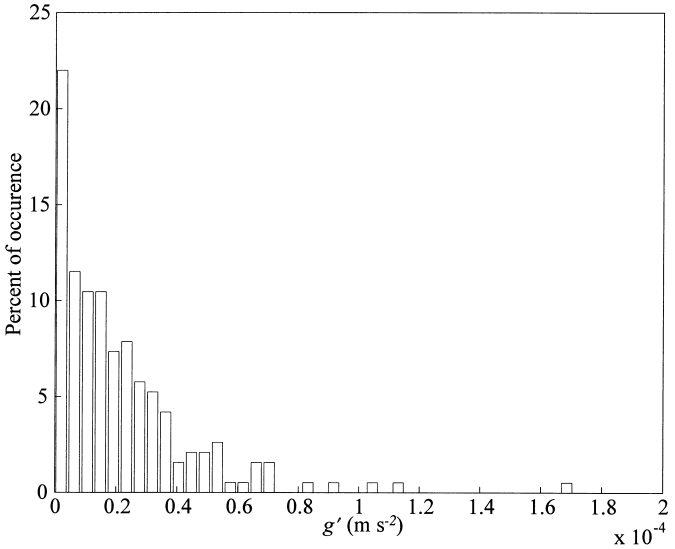

Fig. 8. Histogram of the effective gravity of the segments for the turbulent patches, showing the prevalence of small density fluctuations. g' was derived by subtracting the monotonized density profile from the measured density profile.

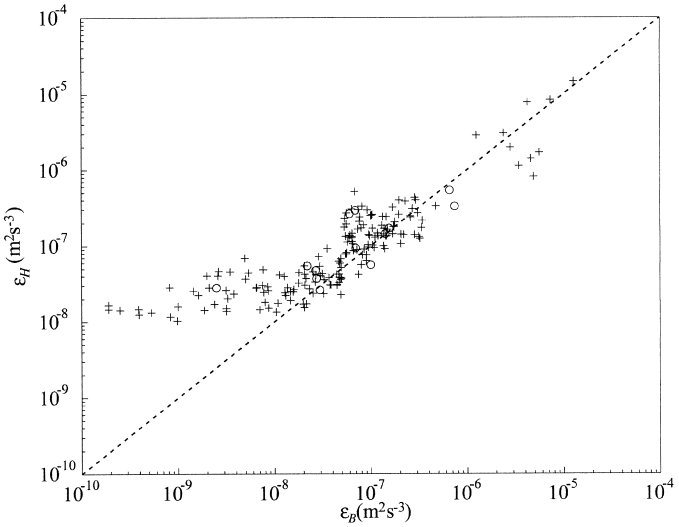

Fig. 9. Dissipation obtained from vertical shear of horizontal velocity versus the simultaneously obtained value from the vertical gradient of temperature, ε_B, showing the correlation between direct and indirect methods when $\varepsilon_B > 10^{-10}$ m^2 s^{-3}. Dadhed line is $\varepsilon_B = \varepsilon_H$. Data points are classified according to the skewness of their centered displacement scale: Sk $\leq$ 1.5 (○) and *Sk* $>$ 1.5 (+).

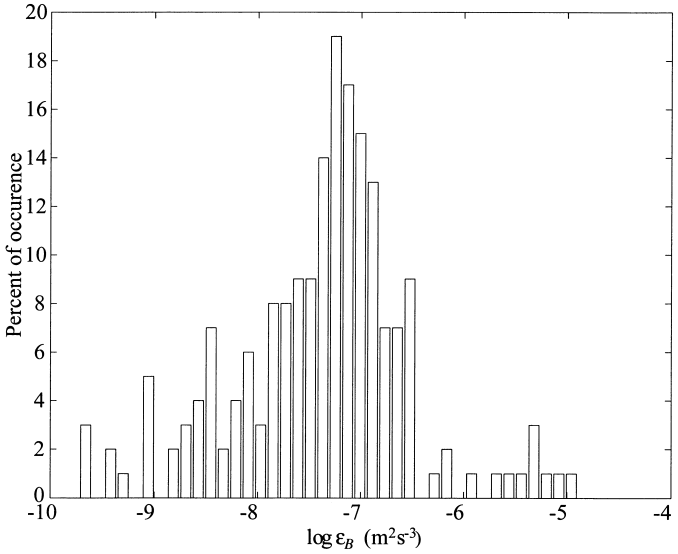

Fig. 10. Histogram of log ε_B for the turbulent segments showing a symmetrical bell-shaped distribution with a mode around 10^{-7} m^2 s^{-3}. Note that the noise level of the instrument is 10^{-10} m^2 s^{-3}, and only values greater than that are plotted. Note that including the nonturbulent segments results in a skewed distribution with a mean value of about 1.5×10^{-9} m^2 s^{-3}.

A comparison between direct and indirect methods of dissipation measurements is shown in Fig. 9, where ε_H is plotted against ε_B. Estimations of Oakey (1982) from relatively longer segments (15 m) showed that these methods agreed for $\varepsilon > 10^{-8}$ m^2 s^{-3}, and our results showed that generally the two methods are not correlated for values of $\varepsilon < 10^{-8}$ m^2 s^{-3}. It appeared that for $\varepsilon_B < 10^{-8}$ m^2 s^{-3}, ε_H was constant, as indicated in Fig. 9. This may be related to the noise of velocity measurements. Assuming $\varepsilon \sim q^3/L_T$, $q_{min} \sim$ 0.0004 m s^{-1} and $L_T \sim$ 0.004 m yields a minimum dissipation of 2×10^{-8} m^2 s^{-3}, which is close to the observed value. Generally, the indirect method performed better and had a lower threshold of 10^{-10} m^2 s^{-3}. Therefore, the indirect estimate of the dissipation was used in all the data analysis below.

Figure 10 shows the distribution of ε_B for all the turbulent segments. The frequency of occurrence was plotted against the logarithm of the dissipation estimates obtained from the temperature gradient signal via Eq. 3. This figure contains all the data that had a dissipation gradient $>10^{-10}$ m^2 s^{-3}. Given this restriction, it appears that the data distribution was nearly lognormal. The maximum likelihood estimator of dissipation was 3.0×10^{-7} m^2 s^{-3}, whereas both the mode and the median were about 5.4×10^{-8} m^2 s^{-3}. These estimates are larger than the values documented in the ocean (e.g., Yamazaki 1990; Gibson 1991), and the average of dissipation corresponded to the Kolmogorov scale of about 2 mm. Therefore, compared to the oceanic values, the dissipation within the turbulent patches was higher, and the overturn scales L_T were smaller.

The intermittency factor $\sigma^2_{\ln \varepsilon} = 3.9$ (Baker and Gibson 1987) was close to the estimated values in the oceanic thermocline (Baker and Gibson 1987; Moum et al. 1989; Gibson 1991) and estuaries (Etemad-Shahidi and Imberger 2000) but was higher than the values derived for the steady shear-driven turbulence in the oceanic surface layer (Moum et al. 1989) and numerical simulations (Ivey et al. 1993). This suggested that in contrast to the turbulence driven by steady shear (which has a low intermittency), turbulence within a lake interior thermocline was more intermittent due to the unsteadiness and intermittent nature of the instability generation mechanisms (*see also* Moum et al. 1989).

Dynamics of the overturns—A great deal has been written about activity signatures of turbulent events (e.g., Gibson 1986; Imberger and Boashash 1986). The simplest of these diagrams is the Fr_t against Re_t representation. Because many investigators (e.g., Yamazaki 1990; Imberger and Ivey 1991) have used $\varepsilon \sim q^3/L_T$ to derive nondimensional numbers, we first examined this relationship by comparing two definitions of the turbulent Reynolds number. As can be seen in Fig. 11, except for the very low values of Re_t, where estimation of q is probably influenced by the resolution of the velocity measurements, the correlation between the two estimates was very good. This means that $\varepsilon \sim q^3/L_T$ can be used wherever velocity measurements are not available and that L_T is a good measure for the most energetic scale of the turbulence. Ore data suggest that $q = 1.3\ (\varepsilon_B L_T)^{1/3}$, which is close to the findings of Ivey and Imberger (1991) but higher than the value suggested by Peters et al. (1995).

In order to compare the two definitions of turbulent potential energy, we plotted the estimate of $N^2L_T^2/2$ against the APEF determined from Eq. 12. This comparison is shown in Fig. 12, where it is seen that the correlation was very good and similar to the oceanic measurements of Crawford (1986), $N^2L_T^2/2$ overestimated APEF by a factor of 3.25.

Using Eqs. 10 and 13 for the definitions of the nondimensional numbers, we plotted the phase diagram of tur-

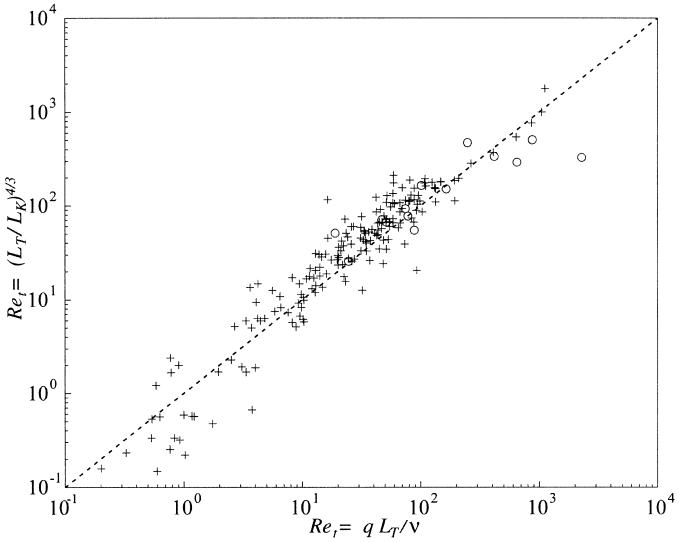

Fig. 11. Comparison between two definitions of the turbulent Reynolds number, showing that both definitions are well correlated, especially for $Re_t > 10$. Dashed line is $q = (\varepsilon_B L_T)^{1/3}$. See Fig. 9 for captions.

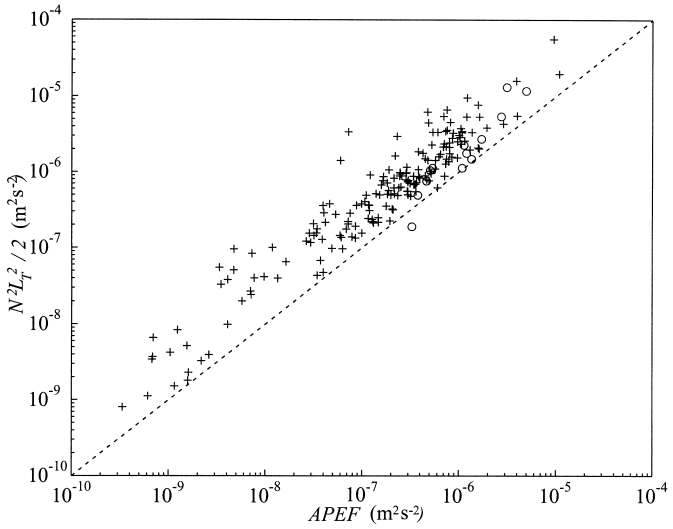

Fig. 12. Comparison between the two definitions of turbulent potential energy, APEF (Eq. 12) and $N^2L_T^2/2$, showing good correlation over four decades. See Fig. 9 for captions.

bulent events in Fig. 13. It is important to remember that each of the data points represents a segment that has an ambient buoyancy frequency (computed from the monotonized density profile) $N > 5 \times 10^{-3}$ s^{-1}, a segment length $>3L_T$, $L_T > 0.001$ m, and a spectra of the temperature gradient that allows unambiguous matching to the theoretical spectra of Eq. 3. The range of the turbulent nondimensional number was similar to the range obtained in other lakes (Imberger and Ivey 1991; Saggio and Imberger 2001). For most of the segments, $Fr_\gamma < 1$ or $Fr_t < 4$, which suggested that most of the turbulent events were not driven by shear instability (Rohr et al. 1988; Imberger and Ivey 1991; Itsweire et al. 1993).

The data points in Fig. 13 were classified according to the magnitude of Sk. In general, the higher skewness was associated with a smaller Reynolds number and an elevated Froude number. Most of the segments with small Sk ($<$1.5) aggregate in the zone of $Re_t > 15$ and $Fr_t \sim 1$; implying active shear-driven events (Ivey and Imberger 1991).

Mixing efficiency and buoyancy flux—We measured the buoyancy flux directly by calculating spatial average of $g/\rho_0(\rho' u_3)$ for each segment. The mixing efficiency or flux Richardson number R_f of Eq. 7 was calculated by using Eq. 3 as an estimate of turbulent kinetic energy dissipation. The distribution of R_f for all turbulent segments is shown in Fig. 14, where the frequency of observation in each bin was nondimensionalized by the total number of observations. The distribution of R_f was symmetrical and bell-shaped; negative efficiencies (due to the dominant U.G. flux) were observed as frequently as positive ones (due to the dominant D.G. flux). The mean and median of R_f were negligible—$\ll$0.17 used in the Osborn (1980) method. A subset of the data with $\varepsilon_B > 10^{-8}$ m^2 s^{-3} was reexamined, and it was found that white noise in the velocity signal had no influence on the statistics of the flux measurements. Oceanic observations of Moum (1990) also showed symmetric distribution of heat flux with a small mean R_f. This was recently confirmed by Moum (1996*a*) and Saggio and Imberger (2000) using extensive dropsonde measurements.

In order to investigate the behavior of the mixing efficiency, we plotted R_f against different nondimensional numbers that are usually used to classify the turbulence. To reduce the scattering and to increase the confidence in the results, values of R_f were binned and averaged for each bin (Fig. 15a,b). The bin-averaged values were again negligibly

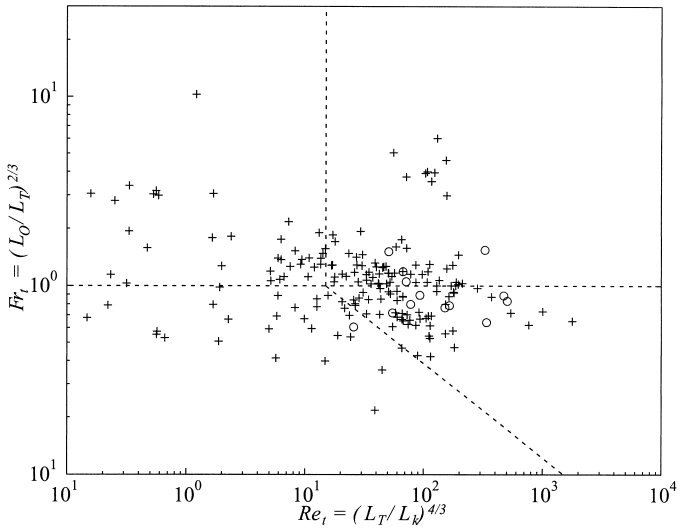

Fig. 13. Phase diagram plot of the turbulent Froude number, Fr_t (Eq. 10) versus turbulent Reynolds number, Re_t (Eq. 13) for individual samples. Vertical dotted line is $Re_t = 15$ (limit of viscosity-dominant regime), the inclined line is $Fr_\gamma = 3.9$, and the horizontal line is $Fr_t = 1$ (transition from inertia-dominant to buoyancy-dominant regime). Note that all the segments in this plot have a dissipation level $>10^{-10}$ m^2 s^{-3} and a $L_T > 0.001$ m. See Fig. 9 for captions.

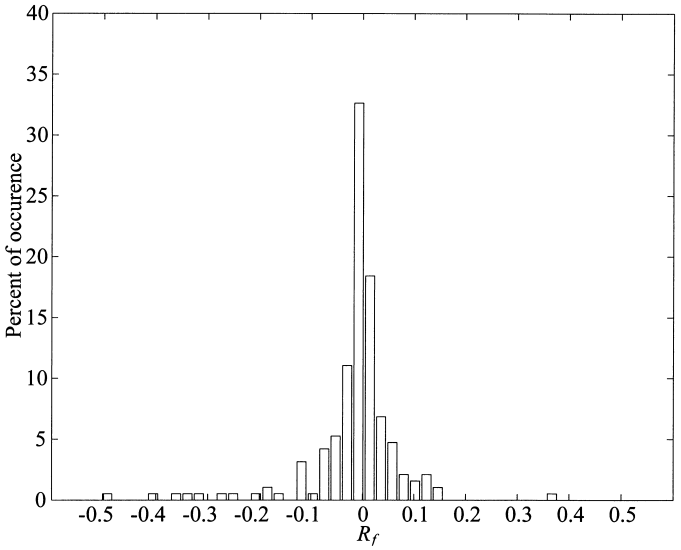

Fig. 14. Histogram of segment-averaged mixing efficiency of flux Richardson number, R_f (Eq. 7), showing a symmetrical bell-shaped distribution with a negligible mean value.

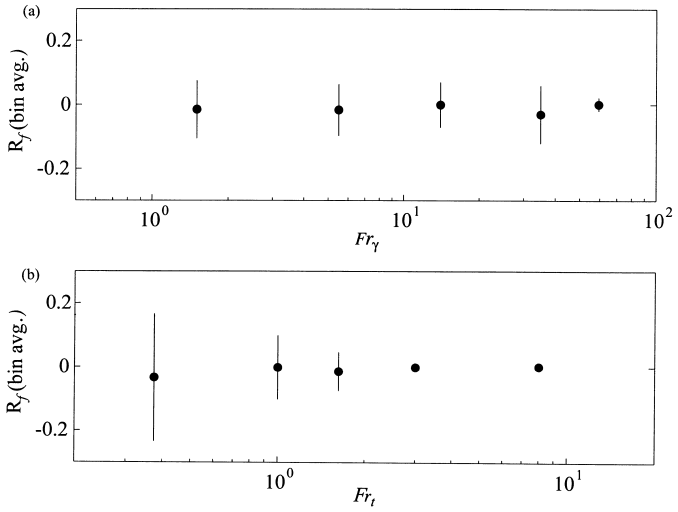

Fig. 15. (a) Bin-averaged R_f versus Fr_γ (Eq. 14). The vertical lines are the error bars. The bin ranges are 0–3, 3–8, 8–20, 20–50, and 50–70. (b) Bin-averaged values of R_f versus Fr_t, showing negligible average mixing efficiency through the whole range. The vertical lines are the error bars, and the bin ranges are 0.0–0.5, 0.5–1.0, 1.0–2, 2–4, and 4–12. See Fig. 9 for captions.

small throughout the range of values shown in Fig. 15a, which does not support the expected critical Fr_γ for suppression or production of buoyancy flux. Furthermore, the many events with low values of Fr_γ indicated that the internal wave–wave interaction played a role in the generation of the observed turbulence (Teoh et al. 1997; Saggio and Imberger 2001). Negative efficiencies were observed even for $Fr_\gamma > 10$, which is greater than the critical value of 4–5. Up-gradient flux at high values of Fr_γ has also been observed in the ocean by Moum (1990, 1996*a*). Such a flux observation implies that even highly energetic events in the thermocline may produce dominant U.G. flux owing to the imposed restrictions of the turbulence generation mechanism.

Figure 15b displays the relationship between R_f versus Fr_t as defined in Eq. 10. The average mixing efficiencies were negligible throughout the range of Fr_t. Ivey and Imberger (1991) predicted a high R_f value at $Fr_t \sim 1$, whereas limited results of direct measurements in lake Argyle (Lemckert and Imberger 1995) and indirect measurements in the ocean (Peters et al. 1995) did not show this behavior. However, Lemckert and Imberger (1998) showed that, in the benthic boundary layer, the bin-averaged values of R_f were a function of Fr_t, and the variation agreed with the proposed formulae of Ivey and Imberger (1991), which could be due to the different flow condition in the boundary layer.

Contributions of the different scales to the buoyancy flux were studied by spectral analysis, which can be used to resolve the scales in which U.G. flux and D.G. flux occur. Figure 16a shows the cospectrum of a segment with $R_f = 0.38$ in a variance preservative form, so the physical area under the cospectrum is proportional to the buoyancy flux. In order to have more confidence, the cospectrum was hand averaged so that points were nearly equally spaced in a logarithmic scale and more samples were averaged at high wave numbers.

Down-gradient flux is associated with a phase angle of zero, which means the density and vertical velocity fluctuation have the same sign; therefore, a particle that has a greater (lesser) density than the background stratification is moving upward (downward). In this segment, D.G. flux was seen at wave numbers between 10 and $5L_K$ (3 and 70 cpm), peaking near a wave number $<50L_K$. A signature of negli-

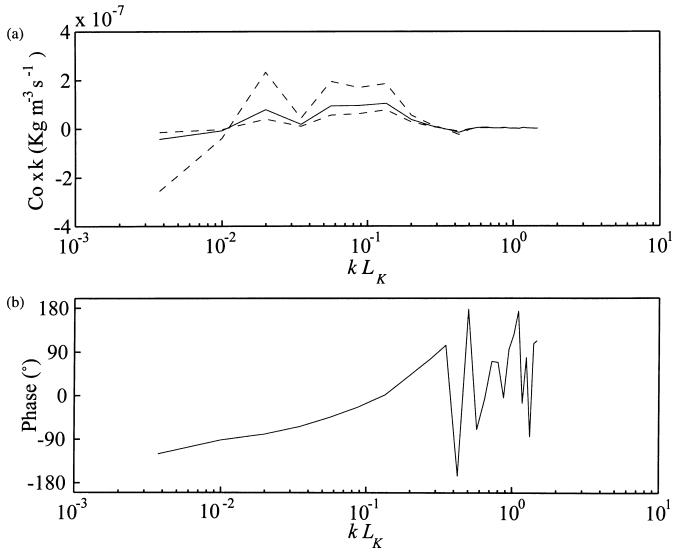

Fig. 16. (a) Cospectra and phase of density and vertical velocity for a segment with positive buoyancy flux as a function of nondimensional wave number in a variance-preserving form, showing dominant down-gradient flux. (b) Phase spectrum. Band averaging was performed so that data points were averaged at higher wave numbers. The length of this segment is 1.45 m, $Re_t = 39$, $Fr_t = 0.2$, and $\varepsilon_B = 2.6 \times 10^{-9}$ m^2 s^{-3}. The dashed lines show the theoretical 95% confidence limits in the estimates.

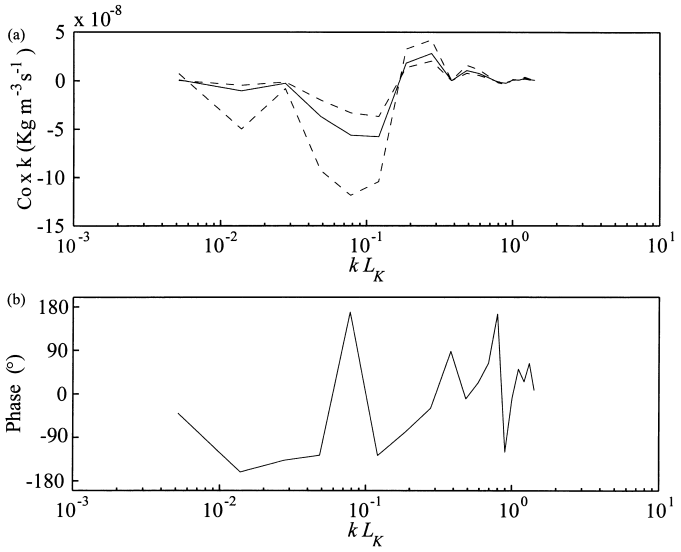

Fig. 17. Cospectra and phase of density and vertical velocity for segment with negative buoyancy flux as a function of nondimensional wave number in a variance-preserving form, showing up-gradient flux at all scales. (a) Band-averaged cospectra in a variance-preserving form. (b) Phase spectrum. The length of this segment is 1.3 m, $Re_t = 291$, $Fr_t = 0.6$, and $\varepsilon_B = 3.5 \times 10^{-9}$ m^2 s^{-3}. The dashed lines show the theoretical 95% confidence limits in the estimates.

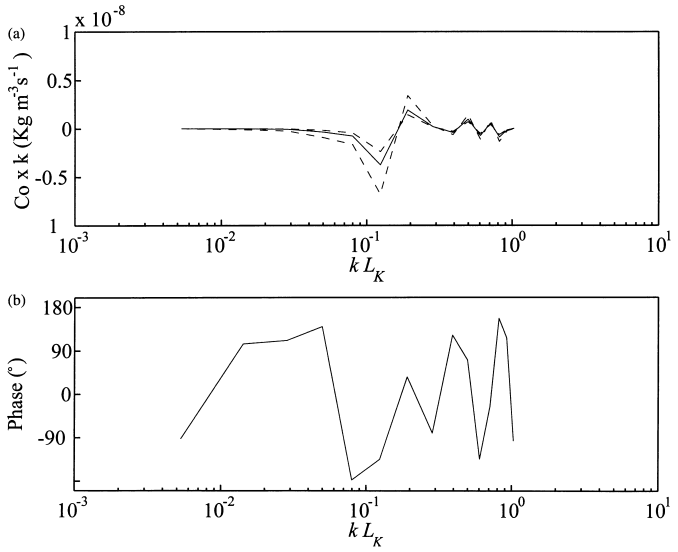

Fig. 18. Cospectra and phase of density and vertical velocity for a segment with negligible buoyancy flux as a function of nondimensional wave number in a variance-preserving form, showing up-gradient flux at small scale and down-gradient flux at large scale compensating each other. (a) Band-averaged cospectra in a variance-preserving form. (b) Phase spectrum. The length of this segment is 1.3 m, $Re_t = 31$, $Fr_t = 1.0$, and $\varepsilon_B = 1.2 \times 10^{-8}$ m^2 s^{-3}. The dashed lines show the theoretical 95% confidence limits in the estimates.

gible U.G. flux existed in wave numbers $<100L_K$. For wave numbers $>5L_K$, which correspond roughly to 50 cpm, the correlation between density and velocity fluctuation became negligible because these fluctuations are negligible in the range of dissipative scales (Yamazaki and Osborn 1993).

By contrast, the cospectrum of another segment with $R_f = -0.33$ is shown in Fig. 17a. Up-gradient flux appeared at large scales of motion where the wave number varied from 200 to $7L_K$ and the peak was at $12L_K$. This behavior is similar to that of decaying flow with strong stratification (e.g., Komori and Nagata 1996). No sign of D.G. flux was observed at large scale and weak mixing was observed at small scale (Fig. 17a). Similar to the previous figure, the flux became negligible at dissipative scales ($3L_K$). This kind of dominant restratification is common in field measurements and has been observed frequently in recent studies (Moum 1990, 1996*a*; Gargett and Moum 1995; Lemckert and Imberger 1995). Cospectrum of another segment with negligible buoyancy flux showed simultaneous D.G. and U.G. fluxes at different scales of motion and not a flat cospectrum with a zero correlation between density and velocity (Fig. 18). This means that zero buoyancy flux or negligible correlation between density and velocity fluctuations is not sufficient for the extinction of turbulence (Lienhard and Van Atta 1990).

In all of the above three figures, the cospectrums did not show noisy behavior and the peaks were significant. This implies that even for segments with low dissipation values, estimated flux was not influenced by the noise in the velocity and/or density measurements. Furthermore, the cospectrums became negligible at wave numbers <320 cpm (32 Hz), indicating that high-frequency noise in the velocity signal has not influenced the calculated flux spectra.

These spectra were three instantaneous realizations and show the statistical nature of buoyancy flux measurement. Even though the profiling was fast enough and the flow could be assumed to be frozen, the buoyancy flux was sampled randomly at different stages of turbulence development. Therefore, these measurements need to be averaged to yield a true estimator of the flux.

Discussion

The nature of density overturns, dissipation, and dynamics of events—The results of our study showed that the overturns in each thermocline were very small, and this finding substantiates the work of Imberger and Ivey (1991), Saggio and Imberger (2001), and Wuest et al. (2000). The temperature (and therefore density) profiles characteristically showed fine perturbations as shown in Fig. 4b and only very rarely well-defined larger overturns. The mean value of the Thorpe scale was 43 mm, and the distribution was highly skewed toward small values (Fig. 5). The events were characterized by the absence of large billows and a large skewness of displacement scales. The few observed large events were characterized by a small value of Sk. Another characteristic of turbulent events was the prevalence of small buoyancy anomalies. The mean of the buoyancy anomalies in the segments was very small (2.1×10^{-5} m s^{-2}), and the distribution was also skewed toward small values. Together, these observations suggested that the generation mechanism of the bulk of the events was not simple shear instability but rather internal wave–wave interaction, as observed in laboratory and field experiments of Teoh et al. (1997) and Saggio and Imberger (2001), respectively.

The turbulent events were very intermittent with high dissipation levels; the maximum likelihood estimator of dissipation was 3.0×10^{-7} m^2 s^{-3}, which was higher than that found in the oceanic thermocline. These highly energetic and intermittent events were associated with very small displacement scales. As a result, high dissipation levels (and q) with small overturn scales produced a wide range of turbulent Reynolds numbers.

The good correlation between $(\varepsilon_B L_T)^{1/3}$ and q showed that ε_B and L_T were good estimators of turbulent characteristics and can be used to estimate q. The independently measured values of q, ε_B, and L_T showed that $q = 1.3\ (\varepsilon_B L_T)^{1/3}$, whereas analysis of laboratory data showed that $q = 2\ (\varepsilon_B L_T)^{1/3}$ (Ivey and Imberger 1991). The constant of proportionality in this scaling depends on three parameters: dissipation, length scale, and velocity scale of the turbulence. In order to compare results from the different published studies, it is important to consider the definition of the parameters used by the investigators, which might explain the differences observed (e.g., Peters et al. 1995; Moum 1996*b*).

Mixing efficiency and buoyancy flux—Turbulent kinetic energy is sustained primarily by the larger scale of motion, and it is traditionally believed that stratification only affects large scales and not small scales in which the energy is dissipated. In nonfield experiments when turbulence was driven by shear and grids, U.G. flux was observed mostly at large scales (e.g., Rohr et al. 1988; Lienhard and Van Atta 1990; Yoon and Warhaft 1990; Jayesh and Warhaft 1991). On the other hand, studies of Holt et al. (1992) and Piccirillo and Van Atta (1997) showed that for high values of Ri_g, U.G. flux can exist at small scales. However, recent laboratory experiments (Huq and Britter 1995) showed that the buoyancy flux is intermittent and consists of equal numbers of D.G. flux and U.G. flux (*see also* McPhee 1992). Our field observations showed that U.G. flux was as frequent as D.G. flux and might exist at any motion. These observations were similar to those of the oceanic thermocline and were due to the coexistence of U.G. flux and D.G. flux in typical turbulent events.

Different ways of data processing may have a first-order effect on the results. To calculate the buoyancy flux, Moum (1996*a*) used a fixed low-pass filter (3.75 m) to resolve vertical velocity fluctuations, whereas in the present study, the displacement length scale was used as the filter size. The latter method is considered to be more appropriate because it is unclear how a fixed filter size could consistently remove all the nonturbulent fluctuations. Moum (1996*a*) did not remove the mean flow from the vertical fluctuations within each patch that may result in the mean velocity (present because of large-scale stirring) being included in the calculation of buoyancy flux. Furthermore, Moum (1996*a*) discarded a large number (60%) of the patches that had a negligible buoyancy flux (low correlation coefficient between density and vertical velocity fluctuations) from his data set even though negligible buoyancy flux is a sufficient, but not necessary, condition for extinction of turbulence (Itsweire et al. 1986; Lienhard and Van Atta 1990).

Considering the above-mentioned differences, we can now compare our estimation of Ri_f (Fig. 14) with those of the oceanic thermocline. Both studies resulted in distributions of mixing efficiency with a negligible net value (*see* Moum 1996*a*; Fig. 6). However, oceanic measurement showed higher absolute values for buoyancy flux, which can be attributed to the above-mentioned differences. The estimations of the nondimensional numbers are not reported in Moum (1996*a*); hence, it is not possible to compare the behavior of mixing efficiency in the oceanic thermocline with the existing results. Nevertheless, knowing that the net value of mixing efficiency was negligible, we speculate that the data from the oceanic thermocline also does not follow the trend observed in the steady laboratory and numerical experiments and are more similar to those discussed here.

It is important to consider the differences between results from field and nonfield studies. In the laboratory and numerical experiments, the turbulence generally was driven by shear or grid in a linearly stratified flow. In addition, the results of the laboratory and numerical experiments were derived from very large sample sizes in steady conditions where energy was continuously fed into the turbulence. By contrast, the events were sampled randomly and the turbulence generation mechanism was unsteady. Therefore, the collected flux data needs to be a significant statistical quantity. Scattering in the field data is inevitable because the results from a vertical profiler are derived from instantaneous realizations of the turbulent events and depend on where and when the probe pierces the intermittent and patchy overturns (Lemckert and Imberger 1995). In addition, the relatively short length of the turbulent patches and intermittency of mixing events contribute to the scattering (Hannoun and List 1988; McPhee 1992; Huq and Britter 1995*a*). If a turbulent event is pierced during its growth, the result would show predominantly D.G. flux, whereas if it is pierced during a collapse, the flux would be predominantly U.G. It was noteworthy that there was no difference between the results obtained from Lake Biwa and Lake Kinneret in this study, which means that the same mechanism dominated the turbulence in both lakes.

The D.G. flux in the thermocline is accompanied by the U.G. flux. Mixing and the associated gravitational collapse and restratification in the thermocline (Sun et al. 1996; Yamazaki 1996; Teoh et al. 1997) produces intrusions that can transport mass and tracers horizontally toward the boundaries and can be transported vertically within the benthic boundary layer and recirculated into the lake's interior (Ledwell et al. 1993). These vertical/horizontal processes may determine the path along which particles move and can have a great influence on the biogeochemistry of the lake.

Conclusions

Turbulence in the thermocline was observed to be intermittent (temporally and spatially) but dissipative, as observed by Saggio and Imberger (2001). Most of the turbulent segments exhibited low values of Fr_γ and fine-grained overturns, and the distribution of the centered displacement scales was highly skewed toward small values. This distribution and intermittency of the generation mechanism of the turbulence resulted in a very low net mixing efficiency.

Moreover, the buoyancy flux typically consisted of both up-gradient and down-gradient fluxes at different scales, and the net vertical mass flux was nearly zero in these lakes. This is corroborated by the more extensive study of Saggio and Imberger (2001), where they showed that because of intermittency and low values of Fr_γ only a small fraction (14%) of the lake Kinneret interior has a vertical eddy diffusivity significantly higher than the molecular value; therefore, the interior vertical flux is negligible.

The intermittency of turbulence and short length of turbulent patches in the thermocline resulted in scattering in the estimated mixing efficiencies. However, the finding showed that the predictions based on steady shear- or grid-driven turbulence is not generally applicable to the thermocline of lakes and that they may overestimate the vertical transport. As predicted by Holloway (1983) and Teoh et al. (1997), our measurements showed that the net buoyancy flux caused by internal wave activity is negligible and much less than that used in the Osborn (1980) method.

The observed intermittency and negligible net efficiency of turbulence within the thermocline of these lakes mean that, in the interior, the mean rate of vertical eddy diffusivity is very low. This finding is in line with recent studies of lakes. Wuest et al. (2000), using different indirect methods, showed that interior mixing was barely above the molecular value, whereas Goudsmith et al. (1997) noted that vertical flux is determined mainly by boundary mixing in small and medium-sized lakes.

All of these findings suggest that the main physical process responsible for the vertical transport of the mass in lakes is boundary mixing and not interior mixing. In fact, Gregg (1987) summarized two scenarios for vertical mixing in the oceanic thermocline: a diffusive thermocline with a large rate of vertical eddy diffusivity and a ventilated thermocline with a small rate of vertical eddy diffusivity. Our results suggested that mixing processes in the thermocline of the lakes can be considered ventilated rather than diffusive. This will influence the path of the suspended and dissolved matter and therefore is implicated in the prediction and simulation of the biogeochemistry of natural water bodies.

References

BAKER, M. A., AND C. H. GIBSON. 1987. Sampling turbulence in the stratified ocean: Statistical consequences of strong intermittency. J Phys. Oceanogr. **17:** 1817–1836.

BATCHELOR, G. K. 1959. Small scale variation of convected quantities like temperature in turbulent field. J. Fluid Mech. **5:** 113–133.

CRAWFORD, W. R. 1986. A comparison of length scales and decay time of turbulence in stably stratified flows. J. Phys. Oceanogr. **16:** 1847–1854.

DAUGHERTY, J. P. 1961. The anisotropy of turbulence at the meteor level. J. Atmos. Terrest. Phys. **21:** 210–213.

DILLON, T. M. 1982. Vertical overturns: A comparison of Thorpe and Ozmidov length scales. J. Geophys. Res. **87:** 9601–9613.

DILLON, T. M., AND D. CALDWELL. 1980. The Batchelor spectrum and dissipation in the upper ocean. J. Geophys. Res. **85:** 1910–1916.

———, AND M. M. PARK. 1987. The available potential energy of overturns as an indicator of mixing in the seasonal thermocline. J. Geophys. Res. **95:** 5345–5353.

ETEMAD-SHAHIDI, A., AND J. IMBERGER. 2000. Anatomy of turbulence in a narrow estuary: Strongly stratified case. J. Geophys. Res.

FLUERY, R. C., AND R. C. LUECK. 1994. Direct heat flux estimates using towed vehicle. J. Phys. Oceanogr. **24:** 801–818.

FOZDAR, F. M., G. PARKER, AND J. IMBERGER. 1985. Matching temperature and conductivity sensor response characteristics. J. Phys. Oceanogr. **15:** 1557–1569.

GARGETT, A. E., AND J. MOUM. 1995. Mixing efficiencies in turbulent tidal fronts: Results from direct and indirect measurements of density flux. J. Phys. Oceanogr. **25:** 2583–2608.

GIBSON, C. H. 1986. Internal waves, fossil turbulence, and composite ocean microstructure spectra. J. Fluid Mech. **168:** 89–117.

———. 1991. Turbulence, mixing and heat flux in the ocean main thermocline. J. Geophys. Res. **96:** 20403–20420.

———, AND W. H. SCHWARZ. 1963. The universal equilibrium spectra of turbulence and scalar field. J. Fluid Mech. **16:** 365–384.

GOUDSMITH, G. H., F. PEETERS, M. GLOOR, AND A. WUEST. 1997. Boundary versus internal mixing in stratified natural waters. J. Geophys. Res. **102:** 27903–27914.

GREGG, M. C. 1980. Microstructure patches in the thermocline. J. Phys. Oceanogr. **10:** 915–943.

———. 1987. Diapycnal mixing in the thermocline. J. Geophys. Res. **92:** 5249–5286.

———, D., E. ASARO, T. SHAY, AND N. LARSON. 1986. Observation of persistent mixing and near-inertial internal waves. J. Phys. Oceanogr. **16:** 856–885.

HANNOUN, I. A., AND J. LIST. 1988. Turbulent mixing at a shear-free density interface. J. Fluid Mech. **189:** 211–234.

HEAD, M. 1983. The use of miniature four-electrode conductivity probes for high resolution of turbulent density or temperature variation in salt stratified water flows. Ph.D. thesis, Univ. of California, San Diego.

HINZE, J. O. 1975. Turbulence. McGraw-Hill.

HOLLOWAY, G. 1983. A conjecture relating oceanic internal waves and small-scale processes. Atmos. Ocean. **21:** 107–122.

HOLT, S. E., J. KOSEFF, AND J. H. FERZIGER. 1992. A numerical study of the evolution and structure of homogeneous stably stratified sheared turbulence. J. Fluid Mech. **207:** 499–539.

HUQ, P., AND R. BRITTER. 1995*a*. Mixing due to grid-generated turbulence of a two-layer scalar profile. J. Fluid Mech. **285:** 17–40.

———, AND ———. 1995*b*. Turbulence evolution and mixing in a two-layer stably stratified fluid. J. Fluid Mech. **285:** 41–67.

———, AND D. STRETCH. 1995. Critical dissipation rate density stratified turbulence. Phys. Fluids **7:** 1034–1039.

IMBERGER, J. 1995. Transport processes in lakes: A review, p. 99–144. *In* R. Margalef [ed.], Limnology now: A paradigm of planetary problems. Elsevier.

———, AND B. BOASHASH. 1986. Application of the wigner-ville distribution to temperature gradient microstructure: A new technique to study small-scale variations. J. Phys Oceanogr. **16:** 1997–2012.

———, AND R. HEAD. 1994. Measurements of turbulent properties in a natural system, p. 1–20. *In* Fundamentals and advancements in hydraulic measurements and experimentation. American Society of Chemical Engineers.

———, AND G. IVEY. 1991. On the nature of turbulence in a stratified fluid, part 2: Application to lakes. J. Phys. Oceanogr. **21:** 660–680.

ITSWEIRE, E. C., K. N. HELLAND, AND C. VAN ATTA. 1986. The evolution of grid generated turbulence in a stably stratified fluid. J. Fluid Mech. **162:** 299–338.

———, J. KOSEFF, D. BRIGGS, AND J. FERZIGER. 1993. Turbulence in stratified shear flows: Implications for interpreting shear-

induced mixing in the ocean. J. Phys. Oceanorgr. **23:** 1508–1522.

IVEY, G. N. 1987. The role of boundary mixing in the deep ocean. J. Geophys. Res. **92:** 11875–11878.

———, AND J. IMBERGER. 1991. On the nature of turbulence in a stratified fluid, part 1 the energetics of mixing. J. Phys. Oceanogr. **21:** 650–658.

———, J. R. KOSEFF, D. BRIGGS, AND J. H. FERZIGER. 1993. Mixing in stratified shear flow: energetic and sampling, p. 335–334. *In* Annual research briefs 1992. Center for turbulence Research, Stanford Univ.

———, J. IMBERGER, AND J. R. KOSEFF. 1997. Buoyancy fluxes in a stratified fluid, p. 311–318. *In* J. Imberger [ed.], Physical processes in lakes and oceans. Coastal and Estuarine Studies, 54. American Geophysical Union.

JAYESH, J. K. Y., AND Z. WARHAFT. 1991. Turbulence mixing and transport in a thermally stratified interfacial layer in decaying grid turbulence. Phys. Fluids **3:** 1143–1155.

JENKINS, W. J. 1980. Tritium and 3He in the Sargasso Sea. J. Mar. Res. **38:** 533–569.

KOLMOGOROV, A. N. 1941. The local structure of turbulence in an incompressible viscous fluid with very high Reynolds number. C. R. Akad. Sci. URSS. **30:** 301–301.

KOMORI, S., AND K. NAGATA. 1996. Effects of molecular diffusivities on counter gradient scalar and momentum transfer in strongly stable stratification. J. Fluid Mech. **326:** 205–237.

LEDWELL, J. R., AND A. BRATKOVIC. 1995. A tracer study of mixing in the Santa Cruz basin. J. Geophys. Res. **100:** 20681–20704.

———, AND A. B. HICKEY. 1995. Evidence for enhanced boundary mixing in the Santa monica basin. J. Geophys. Res. **100:** 20665–20679.

———, AND A. J. WATSON. 1991. The Santa Monica basin trace experiment: A study of diapycnal and isopycnal mixing. J. Geophys. Res. **96:** 8695–8718.

———, A. WATSON, AND C. LAW. 1993. Evidence of slow mixing across the pycnocline from an open ocean tracer release experiment. Nature **364:** 701–703.

LEMCKERT, C. J., AND J. IMBERGER. 1995. Turbulence within inertia-buoyancy balanced axisymmetric intrusions. J. Geophys. Res. **100:** 409–422.

———, AND J. IMBERGER. 1998. Turbulence benthic boundary layers in fresh water lakes, p. 409–422. *In* J. Imberger [ed.], Physical processes in lakes and oceans. Coastal and Estuarine Studies, 54. American Geophysical Union.

LIENHARD, J. H., AND C. VAN ATTA. 1990. The decay of turbulence in thermally stratified flow. J. Fluid Mech. **210:** 57–112.

LUKETINA, D., AND J. IMBERGER. 1989. Turbulence and entrainment in a buoyant surface plume. J. Geophys. Res. **94:** 619–12636.

MCPHEE, M. 1992. Turbulent heat flux in the upper ocean sea ice. J. Geophys. Res. **97:** 5363–5379.

MOUM, J. N. 1996*a*. Efficiency of mixing in the main thermocline. J. Geophys. Res. **101:** 12,057–12,069.

———. 1996*b*. Energy containing scales of turbulence in the ocean thermocline. J. Geophys. Res. **101:** 12,057–12,069.

———. 1990. The quest for k_ρ: preliminary results from the direct measurements of turbulent fluxes in the ocean. J. Phys. Oceanogr. **20:** 1980–1984.

———, D. CALDWELL, AND C. A. PAULSON. 1989. Mixing in the equatorial surface layer and thermocline. J. Geophys. Res. **94:** 2005–2021.

MUNK, W. H. 1981. Internal waves and small-scale processes, p. 264–291. *In* A. Warren and C. Wunch [eds.], Evolution of physical oceanography. V. B. MIT Press.

NAKANASHI, M., T. SEKINO, T. KIMOTO, AND R. TSUDA. 1998. A role of thermocline in relation to plankton distribution of lake Biwa, p. 521–525. *In* J. Imberger [ed.], Physical processes in lakes and oceans. Coastal and Estuarine Studies, 54. American Geophysical Union.

OAKEY, N. S. 1982. Determination of the rate of dissipation of turbulent energy from simultaneous temperature and velocity shear microstructure measurements. J. Phys. Oceanogr. **12:** 256–271.

OKUDA, S., J. IMBERGER, AND M. KUMAGAI [EDS.]. 1995. Physical processes in a large lake, Lake Biwa, Japan. Coastal and Estuarine Studies, American Geophysical Union.

OSBORN, T. R. 1980. Estimation of the local rate of vertical diffusion from dissipation measurements. J. Phys. Oceanogr. **10:** 83–89.

OZMIDOV, R. V. 1965. On the turbulent exchange in a stably stratified ocean. Atmos. Ocean Phys. **8:** 853–860.

PETERS, H., M. C. GREGG, AND T. B. SANFORD. 1995. Detail and scaling of turbulent overturns in the pacific equatorial undercurrent. J. Geophys. Res. **100:** 18,349–18,348.

PICCIRILLO, P. 1993. An experimental study of the evolution of turbulence in a uniformly sheared thermally stratified flow. Ph.D. thesis, Univ. California San Diego.

———, AND C. W. VAN ATTA. 1997. The evolution of a uniformly sheared thermally stratified turbulent flow. J. Fluid Mech. **334:** 61–86.

ROHR, J., AND C. W. VAN ATTA. 1987. Mixing efficiency in stably stratified growing turbulence. J. Geophys. Res. **92:** 5481–5488.

———, E. C. ITSWEIRE, K. N. HELLAND, AND C. W. VAN ATTA. 1988. Growth and decay of turbulence in a stably stratified shear flow. J. Fluid Mech. **195:** 77–111.

SAGGIO, A., AND J. IMBERGER. 1998. Internal wave weather in a stratified lake. Limnol. Oceanogr. **43:** 1780–1795.

———, AND ———. 2001. Mixing and turbulent fluxes in the metalimnion of a stratified lake. Limnol. Oceanogr. **46:** 392–409.

SCHUMANN, U., AND T. GERZ. 1995. Turbulent mixing in stably stratified flow. J. Appl. Meteor. **34:** 33–48.

STILLINGER, D., K. HELLAND, AND C. VAN ATTA. 1983. Experiments on the transition of homogeneous turbulence to internal waves in a stratified fluid. J. Fluid Mech. **131:** 91–122.

SUN, H., E. KUNZO, AND A. J. WILLIAMS. 1996. Vertical heat flux measurements from a naturally buoyant float. J. Phys. Oceanogr. **26:** 984–1000.

TAYLOR, G. I. 1935. Statistical theory of turbulence. Proc. R. Soc. Lond., A **151:** 421–478.

TENNEKES, H., AND J. L. LUMLEY. 1981. A first course in turbulence. MIT Press.

TEOH, S. G., G. IVEY, AND J. IMBERGER. 1997. Laboratory study of interactions between two internal wave rays. J. Fluid Mech. **336:** 91–122.

THORPE, S. A. 1977. Turbulence and mixing in a Scottish loch. Philos. Trans. R. Soc. Lond., A **286:** 125–181.

TOOLE, J. M., K. POLZIN, AND R. SCHMITT. 1995. Estimate of diapycnal mixing in the abyssal ocean. Science **264:** 1120–1183.

WUEST, A., G. PIEPKE, AND D. V. VAN SENDEN. 2000. Turbulent kinetic energy balance as a tool for estimating vertical eddy diffusivity in wind forced stratified waters. Limnol. Oceanogr. **45:** 1388–1400.

YAMAZAKI, H. 1990. Stratified turbulence near a critical dissipation rate. J. Phys. Oceanogr. **20:** 1583–1598.

———. 1996. An observation of gravitational collapse caused by turbulent mixing. J. Phys. Oceanogr. **23:** 826–831.

———, AND T. OSBORN. 1993. Direct estimation of heat flux in a seasonal thermocline. J. Phys. Oceanogr. **23:** 503–516.

YOON, K., AND Z. WARHAFT. 1990. The evolution of grid generated turbulence under conditions of stable thermal stratification. J. Fluid Mech. **215:** 601–638.

Received: 17 July 2000
Accepted: 24 January 2001
Amended: 12 March 2001